THE JOURNAL OF PHYSICAL CHEMISTRY B

Article

pubs.acs.org/JPCB

The Role of the Distal Histidine in H_2O_2 Activation and Heme Protection in both Peroxidase and Globin Functions

Junjie Zhao, Vesna de Serrano, Rania Dumarieh, Matt Thompson, Reza A. Ghiladi, and Stefan Franzen*

Department of Chemistry, North Carolina State University, Raleigh, North Carolina 27695, United States

Supporting Information

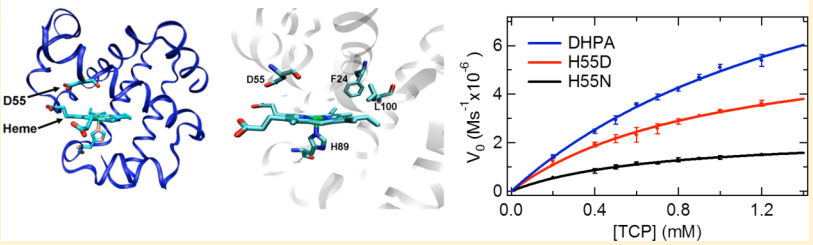

ABSTRACT: The distal histidine mutations of dehaloperoxidase-hemoglobin A (DHP A) to aspartate (H55D) and asparagine (H55N) have been prepared to study the role played by the distal histidine in both activation and protection against oxidation by radicals in heme proteins. The H55D and H55N mutants of DHP A have ~6-fold and ~11-fold lower peroxidase activities than wild type enzyme toward the oxidation of 2,4,6-trichlorophenol (TCP) to yield 2,6-dichloroquinone (DCQ) in the presence of H_2O_2. The origin of the lower rate constants may be the solvent-exposed conformations of distal D55 and N55, which would have the dual effect of destabilizing the binding of H_2O_2 to the heme iron, and of removing the acid−base catalyst necessary for the heterolytic O−O bond cleavage of heme-bound H_2O_2 (i.e., compound 0). The partial peroxidase activity of H55D can be explained if one considers that there are two conformations of the distal aspartate (open and closed) by analogy with the distal histidine. We hypothesize that the distal aspartate has an active conformation in the distal pocket (closed). Although the open form is observed in the low-temperature X-ray crystal structure of ferric H55D, the closed form is observed in the FTIR spectrum of the carbonmonoxy form of the H55D mutant. Consistent with this model, the H55D mutant also shows inhibition of TCP oxidation by 4-bromophenol (4-BP). Consistent with the protection hypothesis, compound ES, the tyrosyl radical-containing ferryl intermediate observed in WT DHP A, was not observed in H55D.

1. INTRODUCTION

Dehaloperoxidase isoenzyme A (DHP A),[1,2] first isolated from the terebellid polychaete *Amphitrite ornata*, is a hemoprotein, which appears to function as both a hemoglobin and a peroxidase. There is a paradox in this combination of functions.[3] To begin with, the oxidation states for the active forms of globins (Fe^{2+}) and peroxidases (Fe^{3+}) are mutually exclusive. In order to function as a hemoglobin, DHP A must cycle between oxy and deoxy states by reversibly binding diatomic oxygen. This function requires ferrous Fe in order to serve an essential role in oxygen storage and transport in *A. ornata*. However, in order to function as a peroxidase, DHP A requires ferric Fe to catalyze the oxidation of 2,4,6-trihalophenol (2,4,6-TXP) to the corresponding 2,6-dihaloquinone (2,6-DXQ) (X = I, Br, Cl, F) using H_2O_2 as a cosubstrate (Scheme 1). An unusual feature of both DHP isoforms, A and B, is that they can both be activated for peroxidase function starting from the oxyferrous form. The activation of oxyferrous heme for exchange by H_2O_2 to initiate reactivity is a unique feature of the dehaloperoxidase-hemoglobin dual function enzymes.[4,5]

Evidence for a true peroxidase function of DHP A and B appears not only in the high catalytic dehalogenation rate of

Scheme 1. Oxidative Dehalogenation of TXP to Yield DXQ as Catalyzed by DHP in the Presence of H_2O_2

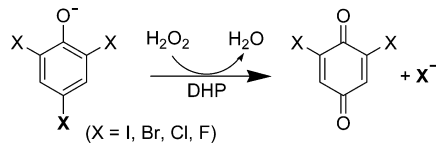

DHP A and B relative to other globins[6,7] but also in the well-defined internal binding site for an inhibitor, 4-bromophenol (4-BP), and specific active site effects in response to binding by 2,4,6-tribromophenol (2,4,6-TBP), the native substrate.[8] In this study, we have investigated another aspect of the paradox in function. Both of the naturally occurring hemoglobin-peroxidase isoenzymes, A and B (DHP A and B), have a conserved distal histidine, H55.[9−13] The distal histidine (His), which is also conserved in nearly all globins and in all heme peroxidases, appears to have nearly opposite structural roles in the classes of proteins. In globins, the distal His stabilizes O_2

Received: January 2, 2012
Revised: July 8, 2012
Published: August 28, 2012

   dx.doi.org/10.1021/jp300014b | *J. Phys. Chem. B* 2012, 116, 12065−12077

binding, and has possible subsidiary functions of preventing autoxidation and discrimination against CO binding to the heme Fe. In peroxidases, the distal His has the nearly opposite role of activating bound H_2O_2 for heterolytic bond cleavage. This function has been studied in DHP A using EPR and ENDOR.[14] Prevention of autoxidation would mean prevention of proton shuttling, since protonation of bound O_2 is the first step in autoxidation of globins. Proton shuttling is precisely the role of the acid−base catalyst in peroxidases. The role of the histidine in protecting the heme and transmitting radicals from the heme in DHP A has been studied by EPR and HYSCORE.[15,16] While mutations that alter the position of the distal histidine can provide some increase in the acid−base catalysis in myoglobin by repositioning the histidine, the reactivity is still far below values typical for peroxidases.[17] Most mutations of the distal histidine strongly decrease the ability of myoglobin to activate H_2O_2 for heterolytic bond cleavage. Similar observations have been made for peroxidases, in which mutations that disrupt the hydrogen bonding pattern surrounding the distal histidine cause a reduction in catalytic rate.[18] Indeed, we have made similar observations in DHP A for the H55V mutation, which has at least 10-fold less activity than the wild type enzyme. The paradox in DHP function[3] centers on the role played by the distal His in DHP, since the dual function of DHP appears to require the performance of two functions that appear to be mutually exclusive. On the basis of these observations, we decided to explore the role of the distal His by mutation to either aspartate (Asp) or asparagine (Asn).

There are few functional amino acids in the distal pocket of DHP aside from the distal His, H55. Like other globins, the distal pocket is essentially entirely hydrophobic. While the position of the distal histidine in DHP A and B is only slightly shifted relative to that observed in most globins, the dynamic flipping of the distal His in and out of the distal pocket is quite different from other globins. This observation led us to hypothesize that the flexibility of the distal histidine is one potentially unique feature of the dual-function proteins DHP A and B.[9] The role of H55 is still a central issue in the studies of peroxidative activity in the dual-function enzyme, since it must play a role in the heterolytic bond cleavage of Fe-bound H_2O_2. On the basis of the X-ray crystal structure data, we have hypothesized that the conformational flexibility of the distal histidine (H55) plays a crucial role in the peroxidase function of DHP.[9] Two conformations of the distal histidine (identified as "open" and "closed") were observed in the room temperature X-ray crystal structure of DHP A (PDB 1EW6),[10,11,19,20] which are correlated with the 5- and 6-coordinate states of heme iron, respectively. The closed conformation is observed when the distal histidine points inside the distal pocket and interacts with a ligand (i.e., water, O_2, or CO) coordinated to the heme iron (PDB 2QFK).[10] The open conformation refers to the state when the distal histidine swings out to a solvent-exposed position (PDB 3DR9). Furthermore, X-ray crystal structures of a series of inhibitors bound in the distal pocket combined with resonance Raman spectra have shown that 4-halophenols (4-XPs) act as inhibitors.[8] The series of inhibitors (4-iodo, 4-bromo, 4-chloro, and 4-fluorophenol) shows a decreasing trend in their binding in the distal pocket that correlates well with their ability to inhibit DHP. This trend is reflected in the decreasing structural localization of the inhibitor in the hydrophobic cavity in the distal pocket (PDB 3LB1, 3LB2, 3LB3, 3LB4)[8] as confirmed by X-ray crystal structures of Xe-derivatized DHP A (PDB 3MOU, 3ORD). The mechanism of inhibition by 4-XPs involves displacement of H55 to the inactive open conformation, which leads to displacement of the Fe-bound water molecule to form a 5-coordinate high spin (5cHS) heme iron.[8] Substrate binding has the opposite effect, "pushing" H55 into the heme pocket and stabilizing bound H_2O as a 6-coordinate high spin (6cHS) adduct.[8] The critical role of H55 has been established in the mutations H55R and H55V, which reduce and abolish activity, respectively.[21]

It is logical to search for mutations that may enhance DHP A activity as a means of understanding the enzymatic mechanism. Given the structural similarity of DHP A and SWMb, it is reasonable to consider the role played by H64 in SWMb[22−26] as a model for H55 in DHPA. H64 has been shown to serve as one of the radical sites of Mb treated by H_2O_2. The instability of compound I in SWMb is attributed to its rapid reduction by the distal histidine through electron transfer.[22,27] However, the accumulation of compound I was demonstrated in the H64D mutant of SWMb when exposed to H_2O_2. This observation was attributed to the >50-fold improvement in the formation rate of compound I. The prolonged lifetime for compound I was also attributed to the mutation of the distal histidine to aspartic acid. For this reason, H64D has the highest peroxidase activity of any mutant of Mb studied thus far.[23,28−30]

On the basis of the unique features of the distal histidine in DHP, as well as the high peroxidase activity of H64D in Mb, it was of interest to investigate the activity of the H55D and H55N mutants in DHP A. Herein we report the preparation, activity, and structure of the H55D mutant of DHP A, which was studied by X-ray crystallography, resonance Raman spectroscopy, and UV−visible stopped flow spectroscopy. The data will show that the H55D and H55N mutants of DHP A have the opposite effect of the H64D mutant of SWMb and are similar to the H42E and H42Q mutants of HRP in their relative activities.[28,31] The comparison of mutant H55D with wild type DHP A addresses the role of the acid−base catalysis in a fundamental sense.

2. MATERIALS AND METHODS

2.1. Materials. Buffer salts were purchased from Fisher Scientific. All other reagents and biochemicals were purchased from Sigma-Aldrich and used without further purification. Deionized water was provided by Barnstead system. The E.Z.N.A Plasmid Mini Kit I was purchased from Omega Biotek, Inc. The QuikChange II site-directed mutagenesis kit was purchased from Stratagene (La Jolla, CA). The required oligonucleotides were synthesized by IDT DNA Technologies, Inc.

2.2. Plasmid Preparation, Protein Expression, Purification, and Preparation. H55D and H55N mutations were generated with the QuikChange II site-directed mutagenesis kit. Mutagenesis [melt (95 °C, 30 s), anneal (55 °C, 60s), and extension (68 °C, 6 min)] was performed for 16 cycles. The plasmid encoding DHP A was used as a template to generate the mutation using the mutagenic primers [5′-G GCC AAG TTC GGT GAT **GAC** ACT GAG AAA GTG TTC AAC C-3′ (forward) and 5′-G GTT GAA CAC TTT CTC AGT **GTC** ATC ACC GAA CTT GGC C-3′ (reverse)], and mutation H55N was generated using the mutagenic primers [5′-G GCC AAG TTC GGT GAT **AAC** ACT GAG AAA GTG TTC AAC C-3′ (forward) and 5′-G GTT GAA CAC TTT CTC AGT **GTT** ATC ACC GAA CTT GGC C-3′ (reverse)]. The plasmids were extracted using the E.Z.N.A plasmid mini kit I. The presence of the desired mutation in the absence of

secondary mutations was confirmed by sequencing. Protein was expressed, purified, and prepared in the ferric form as previously described[16,32] with only minor modification. Deoxyferrous H55D was prepared by mixing the ferric enzyme with sodium dithionite under anaerobic conditions and the H55D-CO complex was prepared by further exposure of the reduced protein to 0.1 atm CO gas.

2.3. UV−Visible Spectroscopy and Enzyme Kinetic Assays. Kinetic and spectroscopic experiments were conducted in 150 mM potassium phosphate (KP_i) buffer at pH 7. UV−visible spectra were collected with an Agilent 8453 UV−visible spectrometer equipped with a temperature control system and Hewlett-Packard UV−visible Chemstation software. The concentration of enzyme in each kinetic sample was 2.4 μM (DHP A) and 12 μM (H55D and H55N). The concentration of substrate TCP was varied from 0.2 to 1.2 mM. The temperature was equilibrated to 20 °C, and a 500-fold excess of H_2O_2 was added to the quartz cuvette to initiate the assay. Spectra were taken every 1 s for 2 min while monitoring the formation of 2,6-DCQ at 273 nm. The initial velocity, V_0, of enzyme turnover was calculated for each concentration of 2,4,6-TCP, and V_0 versus 2,4,6-TCP concentration data were fit independently to the Michaelis−Menten equation using both a linear and a nonlinear fitting function, respectively, in IgorPro5.0 (Wave Metrics Inc.). The inhibition assays were conducted in the presence of 4-BP with different concentrations from 0.1 to 0.8 mM, and spectra were similarly analyzed in Igor Pro5.0.

2.4. Crystallization, Data Collection, and Processing. Crystals were grown by the hanging-drop vapor-diffusion method from 0.2 M ammonium sulfate and 34% polyethylene glycol 4000 at 277 K. The starting protein concentration was 8 mg mL^{-1} in 10 mM Na cacodylate pH 6.5 buffer. In order to obtain crystals of DHP complexed with inhibitor, the protein was incubated on ice for 30 min with the inhibitor (6 mM 4-BP) before being crystallized. Diffraction-quality crystals, which were obtained within 1 week, were cryoprotected by brief immersion in 10 μL of 0.2 M ammonium sulfate solution containing 32% polyethylene glycol 4000 and 15% polyethylene glycol 400, mounted in a nylon loop, and rapidly cryocooled in liquid nitrogen. Data were collected on the SER-CAT 22-ID beamline at the APS synchrotron facility and processed using the HKL2000 program suite.[33] The structure determination and refinement calculations were performed using the CCP4 suite of programs.[34,35] Visualization and manual model building was conducted using Coot model building software.[36] The final models of the H55D and H55D-4BP structures were refined to R/R_{free} values of 22.3/25.5% and 24.1/29.7%, respectively. The H55D model contains two polypeptide chains, three sulfate ions, and 256 water molecules. The H55D-4BP model contains two polypeptide chains, two 4-BP molecules, five sulfate ions, and 299 water molecules. The data-collection and model statistics for the X-ray data sets are summarized in Table 2.

2.5. Resonance Raman Spectroscopy. Protein samples used in the resonance Raman (rR) experiments were prepared and purified as above, and maintained in 100 mM KP_i pH 7 buffer. The final protein concentration for rR samples was 100 μM, and the 4-BP concentration used was 8 mM. The samples were placed into 5 mm diameter glass NMR tubes and stored on ice until needed. Resonance Raman spectra were obtained by Soret band excitation using a Coherent Mira 900 titanium sapphire (Ti:sapphire) laser. The beam was collimated and cylindrically focused to a vertical line of ∼0.5 mm on the sample. The laser power used on the sample was 60 mW focused onto a 100 μm line using a cylindrical lens with an excitation wavelength of 420 nm. The reparation rate was 76 MHz, and the pulse width was 5 ps. Scattered light was collected with a Spex 1877 triple spectrometer (2400 grooves/mm final stage grating) equipped with an ISA SPEX liquid nitrogen-cooled CCD at ∼1.7 cm^{-1} resolution. Computer acquisition of the data was accomplished with SpectraMax 2.0 software. The spectra were calibrated using known peaks from indene standards.

2.6. Fourier Transform Infrared (FTIR) Spectroscopy. The protein sample used in FTIR experiments was maintained in 150 mM KP_i pH 7 buffer with a protein concentration of ∼1.3 mM. The FTIR spectrum was recorded at ambient temperature and averaged over 1024 scans on a Digilab FTS 3000 FTIR spectrometer equipped with a liquid-nitrogen-cooled MCT detector. The protein spectra were recorded with a resolution of 2 cm^{-1} in the range 0−8000 cm^{-1}. Samples were measured in a split cell with CaF_2 windows and a 25 μm path length with H55D-CO and deoxy H55D injected into each half of the cell, and measured alternately so that deoxy H55D provided a background subtraction for the measurement of the CO frequency in H55D-CO.

2.7. Stopped-Flow UV−Visible Spectroscopic Studies. Experiments were performed on a Bio-Logic SFM-400 triple-mixing stopped-flow instrument equipped with a diode array UV−visible spectrophotometer and were conducted at 20 °C in 100 mM KP_i buffer at pH 7. A constant temperature was maintained by a circulating water bath. Data were collected (900 scans in total) over 80 s or 13 min using the Bio Kinet32 software package (Bio-Logic Inc.). Experiments were performed in single-mixing mode, in which H_2O_2 was mixed with ferric H55D. Concentrations after mixing were as follows: [H55D] = 10 μM and [H_2O_2] in the range from 100 μM to 100 mM. All data were evaluated using the Specfit Global Analysis System software package (Spectrum Software Associates).

2.8. Molecular Dynamics Simulations. Molecular dynamic simulations were conducted on both H55D and H55N mutants of DHP A using the NAMD code.[37] The calculation was run using periodic boundary conditions set at the dimensions of the protein molecule dimensions plus an additional 10 Å along each Cartesian coordinate (padding dimension). The cutoff was set to 12 Å with a switching distance of 1.5 Å. The calculations were carried out with frozen hydrogen atoms, which permits a time step of 2 fs/step. Total trajectory lengths were 20 ns. Calculations were performed on the high performance cluster (HPC) at North Carolina State University.

2.9. Density Functional Theory Calculations. Density functional theory (DFT) calculations were carried out for various models of the distal heme interactions shown in Figure 9 using DMol3[38,39] with the generalized gradient approximation (PBE) using the DNP basis set.[40] Calculations were performed on the ARC cluster at NC State University. Structures were geometrically optimized to a convergence of 10^{-6} Hartrees on successive steps in the minimization. The interaction energies of adducts were calculated by displacing H_2O_2 or HOO^- as fragments along a coordinate that represents exit from the enzyme to obtain a potential energy surface (PES) for interaction and binding. The energies used for comparing conformations of charge separated states are the total energies or binding energies of the molecules. The difference in the

energies of two conformers or the difference energies of charge separated states are identical whether the total energy or binding energy is used for the comparison. The PES was obtained by plotting single point energy at displacements along trajectories determined by geometrically optimized end points.

The accepted mechanism for peroxidase enzymatic activation of H_2O_2 involves a rearrangement of the hydrogen atoms on bound H_2O_2 to permit heterolytic cleavage of the O−O bond. The role of the distal amino acid(s) is to remove one of the hydrogen atoms of H_2O_2 to form HO_2^-, which readily binds to ferric iron. The deprotonation of H_2O_2 requires one or more amino acids in the vicinity of the heme to act as the acid−base catalyst, which is first protonated by H_2O_2. Usually the distal histidine is assumed to play this role, perhaps with the help of an accessory arginine residue that is observed in the distal pocket of many peroxidases.[41] The alternative form of activation of H_2O_2 is known as the Fenton mechanism.[42] One can refer to this type of homolytic bond cleavage as a Fenton-type mechanism, since the product is a hydroxyl radical. While a Fenton mechanism is not usually considered in peroxidase chemistry, it is important to compare it to a novel mechanism involving activation of ferrous heme.[43] Recent data suggest that H_2O_2 can displace the O_2 bound to oxyferrous DHP.[5] This displacement would permit an alternative activation mechanism involving a ferrous hydroperoxide intermediate, which must be considered for completeness. Thus, we can distinguish three modes of binding that may be relevant to DHP activation of H_2O_2.

$$Fe^{3+} + HO_2^-(aaH^+) \leftrightarrow Fe^{3+}{-}OOH^- + (aaH^+) \quad (1)$$

where aa represents the distal amino acid.

$$Fe^{3+} + H_2O_2 \leftrightarrow Fe^{3+} - O(H)OH \quad (2)$$

$$Fe^{2+} + H_2O_2 \leftrightarrow Fe^{2+}{-}O(H)OH \quad (3)$$

3. RESULTS

3.1. UV−Visible Spectra of H55D Mutant. The electronic absorption spectrum of ferric H55D [405 (Soret), 507, 539, 641 nm] at pH 7 is presented in Figure 1, and was found to be similar to that of ferric DHP A.[16] The ferric heme spectra are shifted slightly to lower wavelength compared to deoxy DHP A. The UV−visible spectra of deoxyferrous H55D [434 (Soret), 556 nm] and CO-ligated H55D [423 (Soret), 540, 570 nm] at pH 7 are presented in Figure 2. The deoxyferrous and CO-ligated spectra of H55D are both shifted 1−2 nm to higher wavelength than wild type DHP A.[44]

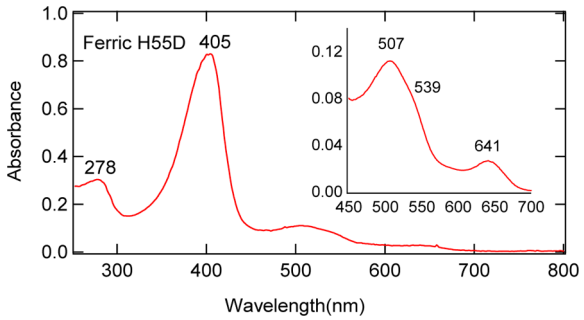

Figure 1. UV−visible spectrum of ferric H55D (~7 μM) in 150 mM pH 7 KP_i buffer. The Soret band is shown at 405 nm, and the Q-band region is shown in the inset.

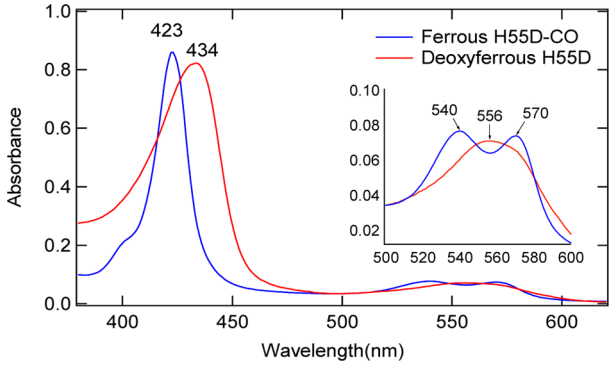

Figure 2. UV−visible spectra of deoxyferrous H55D (~7 μM) (red) and ferrous H55D-CO (~7 μM) (blue) in 150 mM pH 7 KP_i buffer. The Soret bands are observed at 434 and 423 nm for deoxy H55D and H55D-CO, respectively. The Q-band regions are shown in the inset.

3.2. Enzyme Kinetics Study of H55D and H55N. Ferric DHP was evaluated using an assay for peroxidase activity that employed 2,4,6-TCP as the substrate. As observed previously, 2,4,6-TCP is more convenient than 2,4,6-TBP because of its greater solubility.[45,46] Figure 3 shows a comparison of the catalytic rate of wild-type DHP A compared to the H55D and H55N mutant presented in the form of a Michaelis−Menten saturation plot. The kinetic parameters obtained by fitting the curve to the Michaelis−Menten equation are given in Table 1.

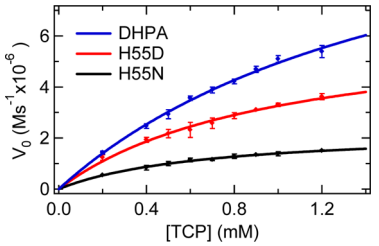

Figure 3. Single wavelength kinetics at 273 nm (DCQ) of the oxidation of TCP by DHP A (blue), H55D (red), and H55N (black) as a function of TCP concentration. Assay conditions were 2.4 μM DHP A, 12 μM H55D or H55N, 0.2−1.2 mM TCP, and 1.2 mM H_2O_2 in 150 mM KP_i buffer at pH 7 at 293 K. The data were fit to a Michaelis−Menten kinetic model shown as the solid lines through the data points.

Table 1. Kinetic Parameters for the Oxidative Dehalogenation of TCP as Catalyzed by Ferric DHP

	DHP A	H55D	H55N
K_M (mM)	1.73 ± 0.15	0.99 ± 0.14	0.68 ± 0.06
k_{cat} (s^{-1})	5.62 ± 0.31	0.54 ± 0.04	0.20 ± 0.01
k_{cat}/K_M (mM^{-1} s^{-1})	3.25 ± 0.33	0.55 ± 0.09	0.29 ± 0.03

For the kinetic measurements, the concentration of H55D and H55N used was 5 times higher than that of DHP A in order to obtain similar values of ΔA (see Figure 3). The K_M values determined for the H55D mutant (0.99 mM) and the H55N mutant (0.68 mM) were slightly lower than that of DHP A (1.73 mM).[47] The comparison of k_{cat} values shown in Table 1 reveals that the catalytic rate was reduced by a factor of ~10

dx.doi.org/10.1021/jp300014b | J. Phys. Chem. B 2012, 116, 12065−12077

and ~28 for H55D and H55N relative to wild type DHP A, respectively. The catalytic efficiency, k_{cat}/K_M, was reduced by a factor of 5.9 and 11.2 for H55D and H55N compared with DHP A, respectively. The effect on k_{cat} is much larger than the effect on K_M, which will be discussed below in terms of the activation of H_2O_2 vs the binding of the substrate to the exterior of the enzyme as two key aspects of the catalytic process.

The oxidation of TCP by H55D in the presence of H_2O_2 can be inhibited by 4-BP (Figure S1, Supporting Information), which is consistent with the inhibition behavior observed in DHP A.[8] The catalytic rate is reduced by a factor of ~2 when the inhibitor concentration is equal to the substrate concentration ([4-BP] = [2,4,6-TCP] = 0.2 mM). Since the kinetics at high 4-BP concentration were not single exponential (Figure S1, Supporting Information), the data were not analyzed further. However, it was evident that the inhibitor has a lower binding affinity than in wild type DHP A. We have shown elsewhere that inhibition is essentially complete when [4-BP] > 2[TCP] in wild type DHP A.[8]

3.3. X-ray Crystallography Study of the H55D Mutant.

The structures of H55D by itself and complexed with 4-BP (H55D-4BP) were determined at 100 K at resolutions of 1.52 and 1.74 Å, and refined to R/R_{free} factors of 22.3/25.5% and 24.1/29.7%, respectively (Table 2). Figure 4A shows the X-ray structure of H55D, in which D55 is in a solvent-exposed conformation outside of the heme pocket. The wild type DHP A room temperature X-ray crystal structure (1EW6) has two

Table 2. Data-Collection and Refinement Statistics for DHP A(H55D) by Itself and Complexed with 4-BP (Values in Parentheses Are for the Highest Resolution Shell)

data collection	H55D	H55D-4BP
wavelength (Å)	0.91339	0.91339
space group	$P2_12_12_1$	$P2_12_12_1$
unit-cell parameters (Å)	a = 57.0, b = 67.9, c = 67.9	a = 58.1, b = 67.6, c = 68.5
resolution (Å)	35.00−1.52 (1.61−1.52)	35.00−1.74 (1.91−1.74)
unique reflections	39120 (6615)	26241 (6936)
completeness (%)	96.5 (97.3)	98.2 (98.6)
R_{merge}[a] (%)	13.4 (43.8)	13.9 (55.5)
$I/\alpha(I)$	5.68 (2.56)	3.38 (2.38)
redundancy	2.8 (2.8)	3.4 (3.5)
refinement		
R_{work}[b] (%)	22.3	24.1
R_{free}[c] (%)	25.5	29.7
no. of protein atoms	2496	2632
no. of solvent atoms	256	299
rmsd from ideal geometry		
bond lengths (Å)	0.0061	0.0076
bond angles (deg)	0.9993	1.0494
Ramachandran plot[d] (%)		
most favored region	94.0	94.4
additional allowed region	5.6	5.6

[a] $R_{merge} = \sum_{hkl}\sum_i |I_i(hkl) - \langle I(hkl)\rangle| / \sum_{hkl}\sum_i I_i(hkl)$, where $I_i(hkl)$ is the ith measurement and $\langle I(hkl)\rangle$ is the weighted mean of all measurements of $I(hkl)$. [b] $R_{work} = \sum||F_o| - |F_c||/\sum|F_o|$, where F_o and F_c are the observed and calculated structure factors, respectively. [c] R_{free} is the R factor for the subset (5%) of reflections selected before and not included in the refinement. [d] Calculated using PROCHECK.[69]

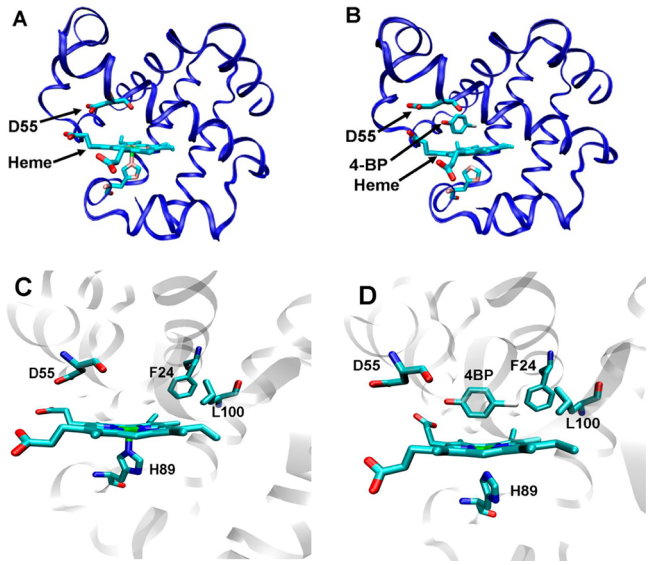

Figure 4. The structure of H55D in the absence (A and C, PDB 3OJ1) and presence of 4-BP (B and D, PDB 3OK5) as determined by X-ray crystallography. Overall folds are shown in A and B, and the active sites are highlighted in C and D. The active site heme group, the proximal and distal histidine residues, and 4-BP (B) are drawn as cyan-colored sticks (only majority conformations are shown).

different H55 conformations.[11] These are known as the "open" and "closed" conformations from comparison with SWMb.[48] In DHP A, these conformations are associated with 5-coordinate deoxyferrous iron (PDB 3DR9) and 6-coordinate metaquo ferric iron (PDB 2QFK), respectively.[9,10]

Overall, the structure of the H55D mutant was found to be very similar to the structure of metaquo DHP A (2QFK). The D55 residue was observed in a solvent exposed conformation in this structure. As was observed previously in the deoxy DHP A structure (3DR9), where the histidine (H55) was in the solvent-exposed conformation, there was no water molecule bound to the heme Fe in the distal pocket in the H55D structure. Although the crystal was prepared in the ferric oxidation state, it was possible that there was reduction of the iron in the X-ray beam as discussed in detail based on observations in both oxy and metcyano DHP A.[10,49] However, regardless of the oxidation state of the iron, this structure follows the trend that Fe ligation of water is associated with the conformation of the distal residue in DHP A.[8,9,50,51] In DHP A (2QFK), a water molecule was present in the distal pocket and H55 was in the closed conformation.[10] Aside from the conformation of the distal residue, there were no other significant differences observed between the structures of WT DHP A and the H55D mutant.

Figure 4B shows the X-ray structure of the H55D-4BP complex, in which 4-BP was found to be located in the distal pocket of H55D. This finding is consistent with the reduced enzymatic activity observed in the H55D kinetic assays in the presence of 4-BP (Figure S1, Supporting Information). Specifically, the internal binding of 4-BP suggests that it can act as an internal inhibitor.[8] The conformation of inhibitor binding is similar in both wild type and the H55D mutant, but the inhibitor is displaced >1 Å toward the exit channel in H55D relative to the wild type enzyme. The distances from heme Fe to the bromine (Br) and hydroxyl oxygen (O) are Fe···Br =

dx.doi.org/10.1021/jp300014b | J. Phys. Chem. B 2012, 116, 12065−12077

5.04 and 5.12 Å and Fe···O = 6.38 and 5.75 Å in wild type DHP A and the H55D mutant, respectively.

3.4. Raman Spectroscopic Study of DHP A (H55D) with 4-BP. The rR spectrum of ferric H55D (Figure 5, blue)

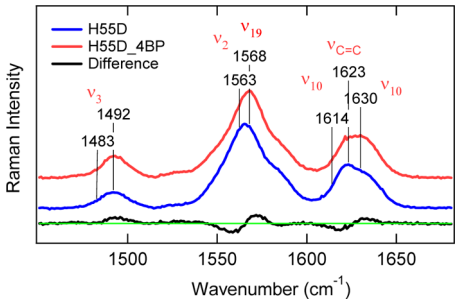

Figure 5. Resonance Raman core size marker band region for ferric H55D (100 μM, blue) and ferric H55D (100 μM) with 4-BP (8 mM) (red). The difference spectrum (red minus blue) is shown by the black line.

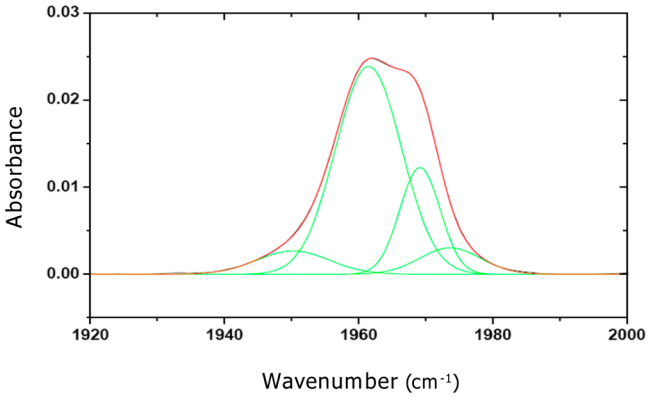

Figure 6. FTIR difference spectrum (black) of CO-ligated H55D at 293 K in 150 mM KP_i buffer at pH 7. Gaussian fitting was performed in Origin Pro (OriginLab Corporation). The overall fitting result is shown in red. The individual peak results (green) are as follows: 1950.2 cm^{-1} (7.9%), 1961.5 cm^{-1} (64.4%), 1969.2 cm^{-1} (20.2%), and 1973.7 cm^{-1}(7.5%).

revealed the presence of both a predominantly 5-coordinate high-spin species (5cHS) (ν_3 at 1492 cm^{-1}, ν_2 at 1568 cm^{-1}, and ν_{10} at 1630 cm^{-1}) and a 6-coordinate high-spin species (6cHS) (ν_3 at 1483 cm^{-1}, ν_2 at 1563 cm^{-1}, and ν_{10} at 1614 cm^{-1}) at room temperature. We note that this may indicate that there is an equilibrium distribution between 5cHS and 6cHS at room temperature. Since the X-ray crystal structure was obtained at 100 K, it is not possible to directly compare the ligation states. However, a similar set of observations has been made for wild-type DHP A, which has an equilibrium distribution of 5cHS and 6cHS at room temperature,[8,50] and 100% 6cHS in the ferric DHP A structure at 100 K (PDB 2QFK).[10] However, in H55D, the equilibrium is weighted toward 5cHS at room temperature and shifts even further toward 5cHS at 100 K, as is evident by the lack of a water molecule bound to the heme iron in the 3OJ1 structure.

With the addition of 4-BP, the ν_3, ν_2, and ν_{10} frequencies shifted from an equilibrium distribution of 5cHS/6cHS to predominantly 5cHS at room temperature. The X-ray crystal structure of H55D with 4-BP (PDB 3OK5), which shows 4-BP in the distal pocket, is consistent as well, since there is no water bound to the heme Fe. The rR spectra were also consistent with the kinetic data and X-ray crystal structure in showing that 4-BP enters the distal pocket and acts as an internally binding inhibitor.

3.5. Fourier Transform Infrared Spectroscopic Study of CO-Ligated Ferrous H55D. At room temperature, DHP A(H55D) exhibited several absorbance bands of heme-bound CO, indicating multiple active site conformations (Figure 6). The dominant band was located at 1961.5 cm^{-1} (64.4%). Minor peaks were located at 1950.2 cm^{-1} (7.9%), 1969.2 cm^{-1} (20.2%), and 1973.7 cm^{-1} (7.5%). In the FTIR spectrum of CO-ligated DHP A, the absorbance bands were found at 1940, 1949, and 1960 cm^{-1}.[44] Both the bands at 1940 and 1949 cm^{-1} are assigned to a heme-CO species with the distal histidine in the closed conformation.[44] The band at 1960 cm^{-1} indicates that the distal histidine is in the open conformation, due to the fact that, when the protonated histidine rotates toward the solvent, the interaction between His55 and the CO ligand is disrupted.[44] By comparing the FTIR spectrum of CO-ligated H55D with DHP A, it is reasonable to assign the band at 1950 cm^{-1} to the closed conformation (~8%) of D55 in H55D. The bands at 1961, 1969, and 1974 cm^{-1} are due to the open conformation (~92%) of D55 in H55D. This result is consistent with the rR result of the ferric form of H55D, which showed an equilibrium between a predominant 5cHS component and a minority 6cHS one at room temperature. Overall, these data indicate that the open conformation is dominant and that the closed conformation of D55 is a minority component.

3.6. Stopped-Flow UV−vis Spectroscopic Monitoring of the Reaction between H55D and H_2O_2. Single-mixing stopped-flow UV−visible spectroscopic methods were employed to probe the activation of H_2O_2 in H55D, and to observe the formation of product, 2,6-DCQ. Figure S2 (Supporting Information) shows the spectral changes that occur within 85 s following the mixing of H55D with 10-fold, 100-fold, 440-fold, and 10 000-fold excess H_2O_2 at pH 7. In all cases, the Soret band was initially observed at 408 nm, similar to that for ferric H55D. There were no spectral changes evident following the addition of 10 equiv of H_2O_2 (Figure S2A, Supporting Information). However, as the H_2O_2 concentration was increased, the Soret band intensity began to show a time-dependent bleaching and a shift to longer wavelength. None of the data exhibited a shift to 420 nm that would indicate formation of a ferryl-containing heme such as compound ES.[16,51] Compound ES was not observed in Figure S2 (Supporting Information) even for concentrations so high that they bleached the Soret band. We investigated whether a radical species was formed under these conditions using rapid-freeze-quench EPR spectroscopy. Wild type DHP A has been shown to form a transient tyrosine radical and oxoferryl intermediate (A_{max} = 420 nm) known as compound ES.[16,52] There was no evidence for such a tyrosyl radical that was assignable in the rapid-freeze-quench EPR measurements conducted using H55D (see Figure S3 in the Supporting Information).

3.7. Molecular Dynamics Study of H55D and H55N. Figure 7 shows the distances between heme Fe and distal residues as determined by MD simulations. The D55 in H55D is oriented toward the solvent and is outside the distal pocket, a result consistent with the X-ray crystal structure. There is no tendency for the negatively charged Asp (D55) to enter the distal pocket, something to be expected on the basis of

dx.doi.org/10.1021/jp300014b | J. Phys. Chem. B 2012, 116, 12065−12077

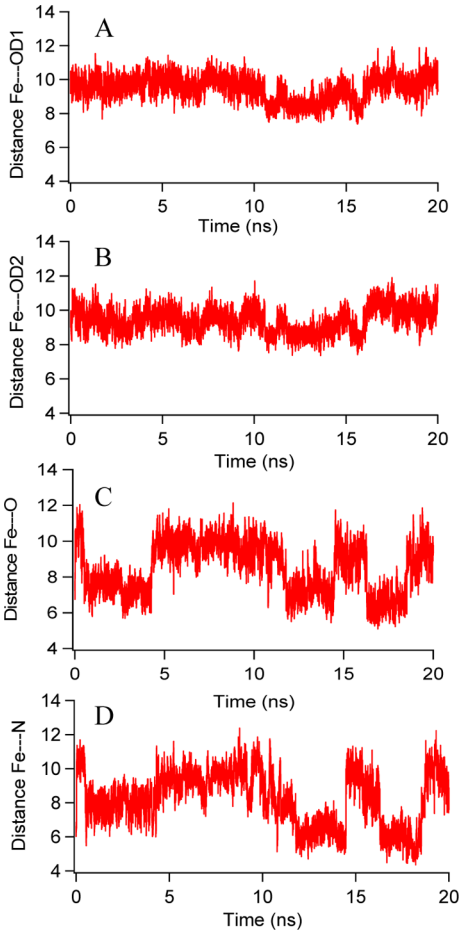

Figure 7. Distances are extracted from a 20 ns NAMD simulation. Heme Fe···Asp55 OD1 in H55D (A), heme Fe···Asp55 OD2 in H55D (B), heme Fe···Asn55 OD1 in H55N (C), and heme Fe···Asn ND2 in H55N (D).

electrostatic considerations. However, N55 in the H55N mutant flips inside and outside the distal pocket, as evidenced by the distances between heme Fe and Asn. The two distinctive conformations of N55 are shown in Figure S4 (Supporting Information). Although we have not conducted a simulation for protonated Asp, we surmise that protonated Asp would have a dynamic trajectory very similar to Asn.

3.8. DFT Modeling of H_2O_2 Activation by DHP A Mutants H55D and H55N. We have considered two alternative mechanisms of activation of H_2O_2 as it enters the distal pockets of the H55D and H55N mutants. These can be described as the Poulos–Kraut[41] and Fenton mechanisms that lead to heterolytic and homolytic bond cleavage, respectively. Further description of the model structures is provided in the Supporting Information. Briefly, geometric optimization of models with H_2O_2 bound to Fe in a porphine model that contain distal asparagine or aspartate can give rise to homolytic cleavage, which can be described as Fe–O(H)···OH. The various geometries and potential energy surfaces associated with homolytic O–O bond cleavage are shown in Figures S5–S14 in the Supporting Information.

In the calculations shown in the Supporting Information, the role of Fe is consistent with known catalysis by a Fenton mechanism, since the HO···OH distance is 1.95 Å, thereby indicating the O–O bond has been broken. This pathway was considered only because homolytic cleavage of H_2O_2 turned out to be energetically favorable for all distal amino acids studied, as shown in detail in Figures S5–S13 in the Supporting Information. Therefore, the focus of the computations was to explore whether the role played by the Fenton pathway could compete with the Poulos–Kraut or heterolytic pathway. As demonstrated in Figure S13 (Supporting Information), homolytic bond cleavage was found to be favorable even when no distal ligand is present. Although these structures with long O–O bond lengths do suggest that an alternative pathway is possible, they may also be part of a Poulos–Kraut mechanism if there is a rearrangement of the H_2O_2 molecule catalyzed by the distal amino acid.

We did not consider all of the possible geometries in the calculations. Rather, the structures were based on the atomic positions obtained from X-ray crystal structures with a fixed β-carbon (see the Supporting Information). While we permitted the distal amino acid to rotate about the β-carbon pivot point, we did not permit the distal amino acid position to shift.

3.8.1. Poulos–Kraut Model. We first consider the implications of the mutation of His → Asp or His → Asn for the Poulos–Kraut mechanism. According to this mechanism, the distal amino acid catalyzes a rearrangement of HOOH to OOH_2, which then can lead to heterolytic bond cleavage along the coordinate O–OH_2. Ultimately, this pathway leads to formation of a ferryl intermediate and H_2O. The results of the trajectories for the H_2O_2 that are centered at the heme Fe and pass in the vicinity of the distal ligand, Asp or Asn, are shown in Figure 8. Since the mechanism involves participation by the

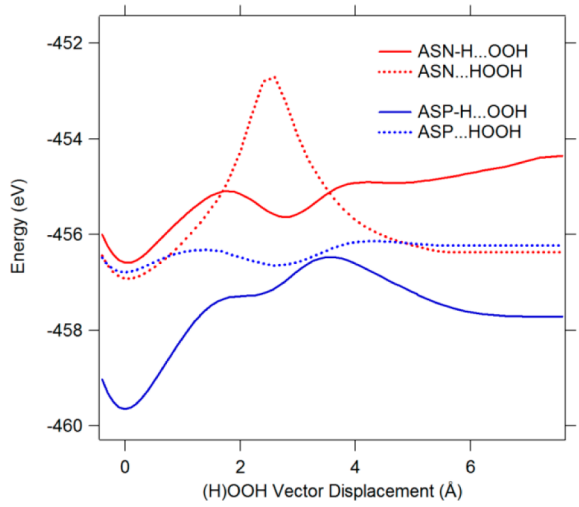

Figure 8. Potential energy surfaces calculated by DFT methods. The potential energy surfaces show the interaction of H_2O_2 with the heme Fe at 0 on the abscissa and the distal amino acid residue ASN or ASP in H55N and H55D, respectively. The trajectories shown correspond to an anionic OOH– (solid) or neutral HOOH (dotted) species entering the distal cavity and passing near the distal amino acid, which is either ASN (H55N) or ASP (H55D). The trajectories are depicted in Figure 9.

distal amino acid as an acid–base catalyst that causes a transient deprotonation of H_2O_2, there are two cases to consider. We can consider the potential energy of a trajectory in which the distal amino acid is protonated and the H_2O_2 is deprotonated to form the peroxide anion HO_2^- following the same trajectory (dotted lines in Figure 8) and a second potential energy surface in which H_2O_2 is intact (solid lines in Figure 8). The molecular geometries of the systems that accommodate HO_2^- and H_2O_2

dx.doi.org/10.1021/jp300014b | J. Phys. Chem. B 2012, 116, 12065–12077

are shown for the ASN model corresponding to the H55N mutant in Figure 9A and B, respectively. The ASP model is

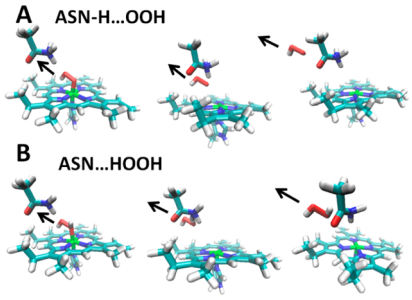

Figure 9. Structures associated with the H55N mutant from the calculation shown in Figure 8. (A) The calculation for OOH^- is shown with a protonated form of the ASN residue. (B) The calculation for neutral HOOH is shown with a normal (unprotonated) ASN amino acid residue.

essentially identical except that the NH_2 of the amide of asparagine is replaced by O in the carboxylate of aspartate. The charges of the systems are +1, 0, 0, and −1 for ASN-H, ASN, ASP-H, and ASP, respectively (see Figures 8 and 9).

Figure 8 shows that there is clearly a bound state at the heme iron for both H_2O_2 and HO_2^-. However, the barrier near the distal residue is significantly different for the two cases. The barrier for H_2O_2 in the vicinity of ASN is the most significant. It is difficult to capture all of the possibilities for proton transfer from H_2O_2 to the distal residue, since the protonated amide group, $(C{=}O)NH_3^+$, which corresponds to ASN-H, rearranges significantly when protonated to accommodate an sp^3 type geometry. The neutral amide group $(C{=}O)NH_2$, which corresponds to ASN, has an sp^2 geometry. Thus, a significant rearrangement needs to occur in order for protonation to take place. No such rearrangement is required for aspartate, since the protonation of the oxygen atom in COO^- to COOH requires only a change in the C—O bond length but no additional changes in structure. There are two clear results from Figure 8. First, HO_2^- is lower in energy than H_2O_2 for the H55D or ASP model, which implies that HO_2^- has a stable trajectory to bind to the heme Fe in that mutant. Second, the ASN model has a barrier to protonation, which impedes acid−base catalysis.

3.8.2. Fenton Model. For the Fenton-type mechanism that involves homolytic bond cleavage, geometric optimization of the Fe(II)-H_2O_2 and Fe(III)-H_2O_2 adducts of heme produced a O−O bond that was significantly elongated relative to either free H_2O_2 or relative to the hydroperoxy intermediate Fe(III)-OOH. This result was obtained irrespective of the oxidation state or the presence of a distal amino acid in the model. Figure 10 shows the potential energy surfaces for the O−O bond in the heme model calculated in the presence of models for the amino acids, aspartate, aspartic acid, and asparagine. These potential energy surfaces can be compared to the same calculation for the HO−OH bond breaking coordinate in heme with no distal amino acid in Figures S12 and S13 and for free H_2O_2 in Figure S14 (Supporting Information). The blue curves in Figure 10 show that homolytic cleavage is spontaneous in these model calculations.

The origin of homolytic cleavage can be understood in terms of the injection of electron density into a π^* antibonding orbital of the O−O system of H_2O_2 by the heme Fe. The bonding of

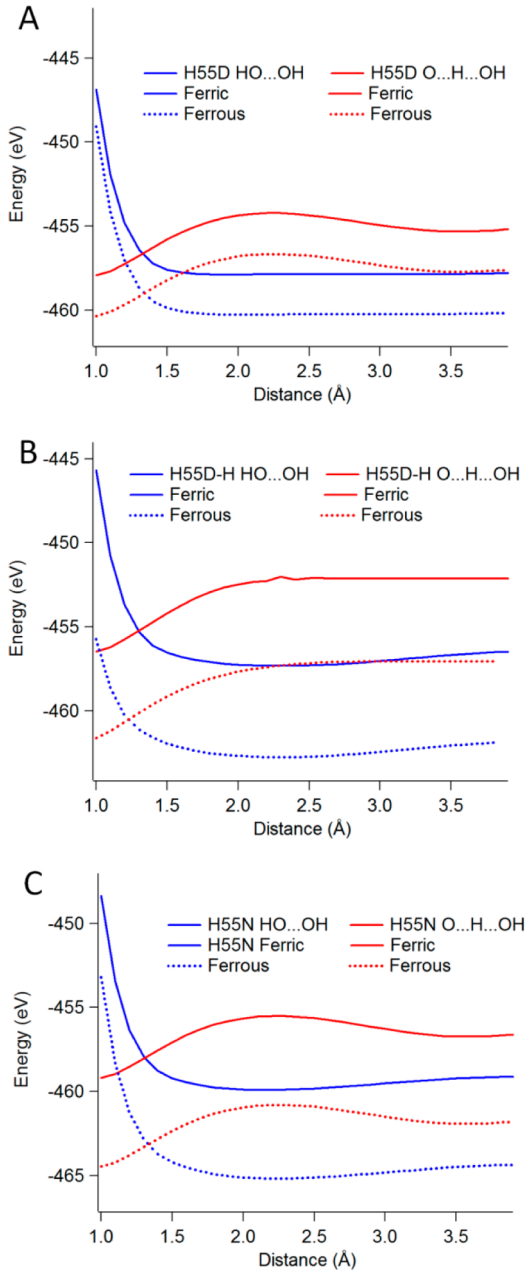

Figure 10. Potential energy surfaces for the ferric and ferrous forms of a heme model which has a Fenton-type activation of H_2O_2 by Fe. The blue curves represent the homolytic bond breaking coordinate for H_2O_2, which can be represented as HO···OH. The red curves represent the displacement of the hydrogen atom from the O(1) atom bound to Fe to the O(2) atom displaced 3 Å from O(1) along the homolytic bond breaking coordinate. This transfer of an H atom can be represented at O···H···OH, and the final structure is O···OH_2.

the aspartate case is the weakest, while shallow potentials are observed for aspartic acid and asparagines. The energies of proton transfer from the Oα atom, bonded to Fe to the Oβ atom, were calculated using two models. Figure 10 also shows a calculation of the projection of the hydrogen atom along a vector from the initial Fe−O(H)−OH geometry to a final Fe−O···OH_2 geometry (red curves). Without a proton transfer step, the HO···OH coordinate would lead to homolytic bond cleavage and Fenton chemistry. Either direct proton or assisted proton transfer via the distal amino acid can result in heterolytic

dx.doi.org/10.1021/jp300014b | J. Phys. Chem. B 2012, 116, 12065−12077

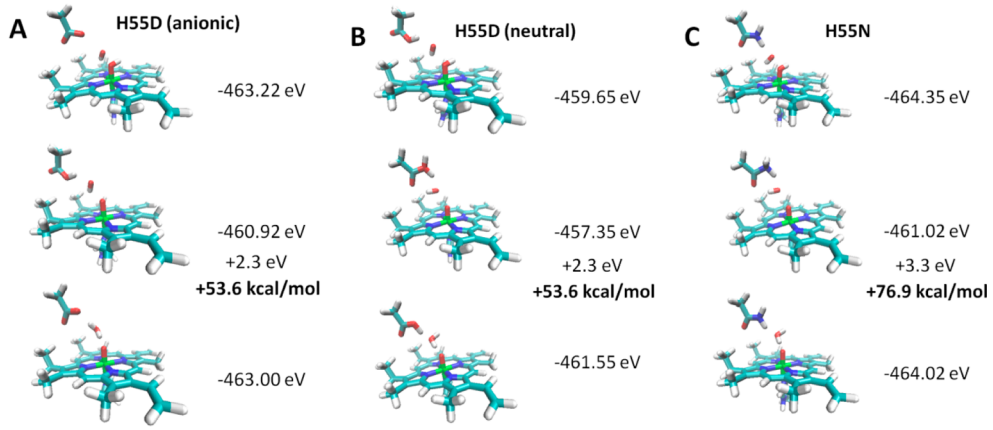

Figure 11. Structures associated with the Fenton-type activation model shown in Figure 10. The limiting chemical forms shown correspond to the homolytic cleavage product (top structures) and the heterolytic cleavage product (bottom structures), which can be indicated as P−Fe−(H)O···OH and P−Fe−O···OH_2, respectively. The energy of the homolytic cleavage product corresponds to the end point for the deoxy species calculation in Figure 10 (blue curve). The energies of the intermediates are lower than the trajectory shown in Figure 10, since the intermediates in this figure consist of protonation of the distal amino acid, i.e., P−Fe−O···(D)H···OH or P−Fe−O···(N)H···OH. (A) The anionic aspartate distal model has a negatively charged aspartic acid, $-CH_2COO^-$, which is transiently protonated to CH_2COOH in the intermediate. (B) The neutral aspartate CH_2COOH is protonated to $CH_2CO(H^+)OH$ in the intermediate state. (C) The amide of asparagine, CH_2CONH_2, is protonated to $CH_2CONH_3^+$.

bond cleavage instead. Direct proton transfer is shown in the calculation in Figure 10, and an alternative path for the rearrangement of the hydrogen atom shown in Figure 11 involves hopping to a lone pair of the distal amino acid. The barrier for proton transfer to result in heterolytic cleavage is clearly lowered by the hopping mechanism. For example, for the H55D anionic calculation, the barrier for the through-space proton transfer is 84.8 kcal/mol (Figure 10), while that for the hopping mechanism via the distal aspartate is 53.6 kcal/mol (Figure 11). The energy lowering effect of the distal aspartic acid (neutral) is even larger, since through space transfer has a barrier of 111.5 kcal/mol (Figure 10) and the protonation of the distal amino aspartic acid has a barrier of 53.6. kcal/mol (Figure 11). Clearly, the distal amino acid can play the role of an acid−base catalyst in the transfer of a proton from one oxygen atom to the other. This catalytic role is analogous the Poulos−Kraut acid base catalysis. Thus, the final structure corresponding to heterolytic cleavage can be achieved in two different ways: (1) rearrangement of the H atom prior to O−O bond breaking or (2) transfer of the H atom subsequent to homolytic O−O bond cleavage.

4. DISCUSSION

The mutation of the distal residue to either aspartate or glutamate has been explored in both globins and peroxidases. The H64D mutant in SWMb led to increased peroxidase reactivity.[23,29] The H42E mutant in HRP has considerably lower activity, but glutamate still has residual acid−base catalytic activity in this mutant.[28,31] Unlike the H55D mutant of DHP A, the glutamate of H42E is located in the distal pocket.[53] The difference in behavior in HRP relative to DHP likely arises from both the neighboring arginine and calcium ligation that can stabilize the negative charge in HRP.[53] The role of an arginine in a globin has also been considered in the T67R mutant of SWMb, which shows an increase of the H_2O_2 activation rate constant by a factor of 2 relative to wild type.[30] However, it is worth noting that neither the H64D nor T67R mutation was found in a random screen for peroxidase function in myoglobin, which suggests that these are not part of the design of mutants that would stabilize compound I formation.[54]

The distal histidine is a very effective acid−base catalyst in part because the histidine pK_a is in the best range to accommodate the transient protonation required for the Poulos−Kraut mechanism. Our work considers the roles of both distal aspartate and asparagine as acid−base catalysts that can activate H_2O_2, as well as the lack of radical formation in H55D, as factors that may explain why the enzymatic turnover of the H55D mutant is ∼6-fold less than wild-type DHP A (Table 1).

There are a number of reasons why D55 may have lower activity than wild type DHP A. The solvent-exposed conformation of D55 may destabilize the binding of H_2O_2 in the distal pocket. Second, D55 may be a poorer acid−base catalyst for activation of H_2O_2 to yield a ferryl intermediate. One test for this hypothesis is the comparison with H55N, which further decreases the rate of acid−base catalysis by a factor of 2 relative to H55D. Third, if H55 does play a role in electron transfer to form compound ES, which is assigned to be the active reaction intermediate in DHP A,[16,51] it is possible that the replacement of the distal histidine by aspartic acid further reduces the peroxidase activity of H55D. On the other hand, if the role of radical formation is protection of the heme under conditions of high turnover, the effect due to loss of radical formation may be small, since the H_2O_2 oxidation activity is also reduced.

The hypothesis that an increased rate of activation of H_2O_2 is coupled with an increased rate of inactivation of the DHP A enzyme is a key aspect of the dehaloperoxidase paradox.[3] There is a fundamental inconsistency in globin and peroxidase functions, which may be resolved by activation of the oxy form of DHP A and/or B. For example, displacement of the bound O_2 by H_2O_2 to initiate peroxidase activity may be a potential route that explains the biological role played by a dehaloperoxidase-hemoglobin.[3,5,55] We systematically survey how these results provide information on the role played by the distal amino acid residue in controlling reactivity in both globins and peroxidases.

The distal histidine in DHP A has a unique role as a gatekeeper for the inhibitor 4-BP. The oxidization of TCP by DHP A is inhibited by the internal binding of 4-BP, which

dx.doi.org/10.1021/jp300014b | J. Phys. Chem. B 2012, 116, 12065−12077

enters the distal pocket, displacing the heme-bound water, and forcing the distal histidine to swing out to the solvent exposed (open) conformation. Attenuated turnover of TCP to DCQ was observed in the presence of a 2:1 ratio of 4-BP to TCP.[8] For H55D, such an inhibition of enzyme turnover was still observed in the presence of 4-BP (Figure S1, Supporting Information). X-ray crystallography (Figure 4B) and resonance Raman spectroscopy (Figure 5) both provide evidence that 4-BP acts as an internal binding inhibitor for H55D in a similar manner. This behavior is consistent with that observed in wild-type DHP A, and it substantiates the hypothesis that the inhibitor, 4-BP, most likely binds as a phenol rather than phenolate. The negative charge of aspartate in H55D would have a very large repulsion with an internally bound phenolate.

Our challenge is to explain why DHP A has an opposite effect from SWMb for a distal His-Asp mutation, and yet we must also explain why DHP A has any activity at all. To explain why the activity of H55D is significantly lower than WT DHP, we first hypothesize that aspartate is poorer as an acid−base catalyst than histidine but still has some activity as observed in the H42E mutant of HRP.[28,31] Unlike the analogous mutant in HRP, our data also suggest that the conformation of D55 observed in the X-ray structure at 100 K (Figure 4) and inferred by the resonance Raman spectrum at room temperature (Figure 5) is mostly, but not 100%, in the solvent exposed conformation. The combination of factors that consists of a comparison with H55N, MD simulations indicating the possibility of the swinging of a distal asparagine or protonated aspartic acid, and DFT calculations that demonstrate the feasibility of acid−base catalysis for aspartate, but not asparagine, suggest an explanation for both the observed inhibitory effects of 4-BP as well as the residual activity of the H55D mutant. However, we note that the MD simulations indicate that aspartate would be found in the distal pocket in the anionic form; thus, the reactivity would be expected to be much reduced relative to the wild type enzyme, as observed. The DFT calculations show that an anionic aspartate would have a significant catalytic effect, acting as an acid−base catalyst as observed in the H64D mutants of SWMb. However, since the distal amino acid appears to have two conformations from both resonance Raman experiments and MD simulations, and is weighted heavily toward the external conformation, we conclude that these factors explain the reduced reactivity of the H55D mutant and the relative similarity of H55D and H55N kinetics. As discussed in previous work, the key to reactivity in DHP is once again shown to be the flexibility of the distal histidine, H55, that we have noted in a series of prior studies.[3,8−10,51]

The distal amino acid, H55, plays multiple roles in heme proteins, with specific functions applicable to both the peroxidase and the globin functions. In globins, the distal histidine (H55) is the primary residue responsible for the stabilization of ligand binding to the heme iron. As observed in other globins, H55 of DHP A interacts with bound O_2 (PDB 2QFN). On the other hand, with respect to the enzymatic activity of DHP A, H55 plays a crucial role in the overall two-electron oxidization of TCP to DCQ in the presence of H_2O_2. Unlike other heme-containing peroxidases,[41,56−61] H55 must act alone as a general acid−base catalyst in DHP A without any supporting hydrogen bonding, such as that from the accessory arginine near the distal histidine that participates in the steps that lead to cleavage of the O−O bond in H_2O_2 by catalyzing a rearrangement of the hydrogen atoms.[50] H55 also stabilizes ligands bound to the heme iron.[9] Thus, the closed conformation of the distal histidine plays a crucial role by placing H55 in the proper geometry to act as a general acid−base catalyst. The 2QFK X-ray crystal structure is thought to represent the active conformation in which the distal amino acid interacts with a heme-iron-bound ligand.[10] However, in the H55D mutant, D55 is in the open conformation and the heme Fe is 5-coordinate. The correlation of the distal residues in the open (solvent exposed) conformation and 5-coordinate heme iron is consistent with the deoxy DHP A X-ray crystal structure (PDB 3DR9).[9] According to our hypothesis, the H55 conformation is strongly correlated with H_2O binding in ferric DHP A such that it is in the internal (closed) conformation when H_2O is bound to the heme-iron (6cHS) and in the external (open) conformation when the heme-iron is 5cHS.[8,10,50] Ligand stabilization likely also extends to H_2O_2, which may facilitate the peroxidase function as well by forming a hydrogen bond with H_2O_2 bound to the heme iron. Therefore, the open conformation is also consistent with reduced peroxidase activity relative to wild type DHP. The H55D mutant eliminates these interactions and appears to destabilize both H_2O and H_2O_2 binding based on the data we have obtained.

The H55 residue may also have the potential to act as an electron transfer intermediate in the peroxidase reaction cycle. The formation of compound ES may rely on electron transfer from one of the tyrosines to the heme by means of H55 as an intermediate on the electron transfer pathway. In Mb, the distal histidine (H64) has been shown to play a role as a conduit for radicals when the protein is treated with H_2O_2.[27,62] One outstanding question in both globin and peroxidase chemistry is what role is played by protein radicals. It may not be possible to generalize for all enzymes, but it appears that type III peroxidases that oxidize phenolic substrates may have reduced activity due to formation of tyrosine or tryptophan radicals. For this reason, the H64D SWMb mutant may give rise to increased oxidation rates because of a reduction in competing formation of protein radicals. Similar considerations apply to catalase-peroxidases, where the initial two radicals formed lead to an autocatalytic formation of a Met-Tyr-Trp cross-linked species, which plays a role in permitting catalase activity.[63,64] While this hypothesis remains to be tested in detail, it is clear that this behavior is quite different from peroxidases such as C*c*P, in which the initially formed tryptophan radical in compound ES is on the electron transfer pathway to the substrate cytochrome *c*.[65,66] The difference in the mechanisms may depend on the distance required for electron transfer.

Another important reason for enhanced peroxidase activity in H64D SWMb is the ∼50-fold faster formation of compound I due to the H64 → D replacement.[23] Studies have shown that H64 enhances the binding of H_2O_2 to the heme iron but does not accelerate heterolytic O−O bond cleavage.[25] The activation of both H_2O_2 binding and heterolytic bond cleavage has been attributed to acid−base catalysis by the distal histidine. Activation of binding refers to the fact H_2O_2 itself binds rather poorly to the heme Fe, while deprotonated HOO^- binds with much greater affinity.[41] Thus, the Poulos−Kraut mechanism involves a deprotonation of H_2O_2 prior to ligation to the iron following the rearrangement to form the $O-OH_2$ isomer, which primed for heterolytic bond cleavage. Aspartate is a poorer acid−base catalyst than histidine, simply based on a model that the best acid−base catalyst will have a pK_a nearly

equal to the pK_a of the donor and acceptor involved in the catalysis.

The series of steps that lead to heterolytic bond cleavage can be expressed by the following equilibria:

$$H_2O_2 + B: \rightarrow HOO^- + B{:}H^+ \quad (1A)$$

$$Fe^{3+} + HOO^- \rightarrow Fe^{3+}{-}OOH^- \quad (1B)$$

$$Fe^{2+}{-}OOH^- + B{:}H^+ \rightarrow Fe^{3+}{-}OOH_2 + B: \quad (1C)$$

The tuning of the acceptor (base) and donor (acid) ability of the catalyst B: is the key to catalysis in this mechanism. Histidine has a pK_a of ∼6.0, which is both close to the ambient pH in the cell (pH ∼ 7.4) and relatively close to that of bound peroxide. The pK_a of free H_2O_2 is ∼11.7. However, when H_2O_2 is bound to iron, the pK_a is likely shifted significantly lower and hence closer to equivalence with the pK_a of histidine. Aspartate, on the other hand, has a pK_a of ∼4.7. While there is some possible further effect of the protein electrostatic environment on the pK_a of both histidine and aspartate, this effect is likely to be minor in the hydrophobic cavity of the distal pocket. These considerations imply that the acceptor ability of aspartate (base activity) is not as well tuned to the rearrangement reaction that ultimately precedes the O−O bond cleavage of a ferric-hydroperoxide precursor. For this reason, the mutation of the distal residue to aspartic acid may result in a lower activity in DHP A, which is a different behavior than the analogous mutant in SWMb.

The role played by the distal aspartate as a potential acid−base catalyst can be understood by comparison with the H55N mutant, both in MD simulations and DFT calculations. The MD simulations (Figure 7) show that a neutral amino acid has some residence inside the distal cavity, which suggests that a protonated aspartic acid would be able to enter the distal cavity. This is important because it suggests that aspartate can play a role as an acid−base catalyst in the proper conformation in the distal pocket, albeit transiently deprotonated while in the distal pocket. The DFT calculations (Figure 8) show that aspartate has an appropriate energetic profile to act as a Poulos−Kraut intermediate that can deprotonate H_2O_2 to HOO− on its trajectory into the distal pocket. Thus, the scenario given in Scheme 1, which is required for the Poulos−Kraut mechanism, is fulfilled for H55D according to the energetic profile in Figure 8. However, H55N is not activated according to the calculated potential energy surface shown in Figure 8, and this explains the observation that the H55N mutant has negligible activity, while H55D still has residual activity approximately 10 times lower than wild type. Finally, Figures 9 and 10 show that aspartate may also play a role in the activation of H_2O_2 bound to ferrous Fe in an unusual mechanism, recently observed in DHP B.[43]

In wild type DHP A, evidence for compound ES is found in UV−visible spectroscopy with the formation of the signature spectrum for a ferryl intermediate (an observed shift of the Soret band to ∼420 nm), and more directly in freeze-quench EPR spectroscopic measurements.[16] However, for H55D, no transient ferryl-containing species (neither compound II nor compound ES) was observed at H_2O_2 concentrations typically employed to observe this intermediate (Figure S3, Supporting Information). The mutant underwent heme bleaching at higher H_2O_2 concentrations (Figure S2C and D, Supporting Information). The bleaching suggests that there is even less protection of the heme against oxidation by H_2O_2 than in wild type DHP A. This would be consistent with a lack of protein radicals, since protein radicals have been postulated to have a protective effect. The lack of compound ES formation was confirmed by rapid-freeze-quench EPR methods, which showed no protein radicals were formed in the H55D mutant in distinction to wild type enzyme[16,51] (Figure S3, Supporting Information).

A combination of X-ray crystallography and resonance Raman spectroscopy explains the multiple conformations of the aspartate in H55D. Of course, the reference for this work is the wild type DHP A structure and resonance Raman spectra. It is known from the X-ray crystal structure (PDB 3OJ1) that D55 adopts a 100% solvent-exposed conformation (open) in H55D at 100 K. It is not possible to predict the room temperature conformation of the distal residue from this low temperature X-ray crystal structure. The role of temperature as a determinant of the ligation state equilibrium (5cHS/6cHS) in wild-type DHP A has been established previously.[9] The room temperature X-ray crystal structure of DHP A (PDB 1EW6) shows that the distal histidine adopts two conformations, internal (closed) and external (open), with occupancies of 60 and 40%, respectively. As mentioned above, closed and open conformations are correlated to 6cHS and 5cHS heme states, respectively. Resonance Raman spectroscopy has revealed that DHP A has an equilibrium distribution of 6cHS (∼60%) and 5cHS (∼40%) at room temperature, which is consistent with the room temperature X-ray crystal structure. However, at 100 K, H55 adopts a 100% closed conformation in the ferric DHP A structure (PDB 2QFK).[11] Therefore, it is reasonable to suggest that there is a minority percent of D55 adopting a closed conformation and serving as an acid−base catalyst at room temperature, which results in the lowered enzymatic activity of the H55D mutant. This was shown both by the resonance Raman (Figure 5) and FTIR spectroscopy (Figure 6). The resonance Raman spectra, obtained at room temperature, indicate an equilibrium between 5cHS (predominant) and 6cHS hemes, correlated to open and closed conformations, respectively. The FTIR spectrum, also obtained at room temperature, indicates an equilibrium between a predominantly open conformation (∼92%) of D55 and a minor closed conformation (∼8%).

The DFT calculations led to consideration of a Fenton-type mechanism for activation of Fe-bound H_2O_2. This consideration was prompted by the fact that a geometry optimized structure with bound H_2O_2 had an elongated bond. However, the Poulos−Kraut mechanism involves deprotonation of H_2O_2 during its approach to the heme Fe. This important distinction leads to a bound peroxy form that lacks one of the protons. Thus, while we have considered the Fenton mechanism for completeness, the calculations are consistent with the traditional Poulos−Kraut mechanism in both wild type and mutants.

5. CONCLUSION

In order to study the role played by the distal histidine, a globin-peroxidase, we have prepared the H55D and H55N mutants of DHP A. The H55D mutant is analogous to the H64D mutant of SWMb, which is the most active peroxidase of any Mb mutant studied to date. However, unlike H64D in SWMb, the H55D mutant is not a better peroxidase but instead has ∼6-fold lower activity than wild type DHP A. The X-ray crystal structure shows that D55 adopts a solvent-exposed conformation at 100 K with no detectable conformation in the internal site at that temperature. Analysis of the room

temperature resonance Raman and FTIR spectroscopic studies suggests open (~92%) and closed (~8%) conformation occupancies at room temperature for D55, rather than the 60%/40% closed/open ratio observed for the native H55. The hypothesis that a protonated form of the aspartate could enter the distal pocket is consistent with MD simulations of H55N, in which asparagine serves as a model for protonated aspartic acid. The favorable energetics of protonation of aspartate by H_2O_2 have been shown by DFT calculations. Thus, a mechanistic interpretation of the role played by distal aspartate is that the ca. 8% of D55 observed in the closed conformation may explain why the H55D mutant has residual peroxidase activity. The fact that H64D increases peroxidase activity in SWMb may be a consequence of the electrostatic environment of a globin that is adapted for oxygen transport and has a very low rate, and even lower yield for peroxidase chemistry. Thus, the fact that the distal histidine in DHP is poised for effective acid–base catalysis may explain why DHP more closely resembles the His → Glu (H42E) mutant in HRP, rather than H64D in SWMb.

While aspartic acid is a poorer acid–base catalyst than histidine based upon pK_a considerations, comparison with HRP suggests that it should have some activity. However, the distal amino acid has a second function, which is to act as a conduit for formation of protein radicals. We have suggested that these radicals are off pathway for peroxidase activity, since formation of a phenolate radical clearly competes favorably when TCP is present as a substrate.[67] The lower activity of H55D may then also be related to the fact that solvent-exposed D55 cannot efficiently transfer radicals to the tyrosine residues of DHP A.[16,51] If radical formation competes with activity in SWMb but not in DHP A, then the role played by the H64D mutant is mainly that of a decrease in the formation of competing radicals. When substrate is present, it competes with tyrosine radical formation. This view is consistent with a large number of tyrosine mutants that have been made in DHP A.[3,16,21,51] When the protein radical pathway is not available, reactive heme radicals can form, which leads to alteration of the heme as compound RH and ultimately to heme cross-linking to the globin.[16,51] Heme degradation can also occur because of lowered activity of the distal amino acid. When the rate of compound I (or compound ES in DHP) slows sufficiently, the heme can begin to degrade by a heme oxygenase pathway.[68] Consistent with these observations, heme degradation is more rapid in H55D than in wild type DHP. In conclusion, the H55D and H55N mutations of DHP demonstrate the multiple functions of the distal histidine, which can be summarized as a catalytic function as an acid–base catalyst, a stabilizing function for diatomic oxygen ligand binding and a protective function to prevent radical and chemical attack of the heme.

■ ASSOCIATED CONTENT

Supporting Information

Single wavelength inhibition kinetics are shown. Spectra of the heme of DHP A exposed to differing concentrations of H_2O_2 are shown. Data obtained from a freeze-quench EPR study is presented. Figures showing structures used in DFT calculations are presented. Methods used for determining DFT models are discussed. This material is available free of charge via the Internet at http://pubs.acs.org.

■ AUTHOR INFORMATION

Corresponding Author

*E-mail: Stefan_Franzen@ncsu.edu. Phone: 919-515-8915.

Notes

The authors declare no competing financial interest.

■ ACKNOWLEDGMENTS

S.F. and R.G. gratefully acknowledge support through Army Research Office grant 57861-LS. S.F. thanks Dr. B. Delley for access to the DMol3 code used in these calculations.

■ ABBREVIATIONS

dehaloperoxidase-hemoglobin isoenzyme A (DHP A) and B (DHP B); sperm whale myoglobin (SWMb); horseradish peroxidase (HRP); horse heart myoglobin (HHMb); 2,4,6-trihalophenol (2,4,6-TXP); 2,6-dihaloquinone (2,6-DXQ) (X = I, Br, Cl, F); 2,4,6-trichlorophenol (TCP); 2,6-dichloroquinone (DCQ); 4-bromophenol (4-BP); distal histidine in DHP A (H55); distal histidine in SWMb (H64); resonance Raman (RR); 5-coordinate high spin (5cHS); 6-coordinate high spin (6cHS)

■ REFERENCES

(1) Weber, R. E.; Mangum, C.; Steinman, H.; Bonaventura, C.; Sullivan, B.; Bonaventura, J. *Comp. Biochem. Physiol., Part A* **1977**, *56*, 179.
(2) Chen, Y. P.; Woodin, S. A.; Lincoln, D. E.; Lovell, C. R. *J. Biol. Chem.* **1996**, *271*, 4609.
(3) Franzen, S.; Thompson, M. K.; Ghiladi, R. A. *Biochim. Biophys. Acta* **2012**, *1824*, 578.
(4) Du, J.; Sono, M.; Dawson, J. H. *Biochemistry* **2010**, *49*, 6064.
(5) D'Antonio, J.; Ghiladi, R. A. *Biochemistry* **2011**, *50*, 5999.
(6) Osborne, R. L.; Coggins, M. K.; Walla, M.; Dawson, J. H. *Biochemistry* **2007**, *46*, 9823.
(7) Belyea, J.; Gilvey, L. B.; Davis, M. F.; Godek, M.; Sit, T. L.; Lommel, S. A.; Franzen, S. *Biochemistry* **2005**, *44*, 15637.
(8) Thompson, M. K.; Davis, M. F.; de Serrano, V.; Nicoletti, F. P.; Howes, B. D.; Smulevich, G.; Franzen, S. *Biophys. J.* **2010**, *99*, 1586.
(9) Chen, Z.; de Serrano, V.; Betts, L.; Franzen, S. *Acta Crystallogr., Sect. D* **2009**, *D65*, 34.
(10) de Serrano, V.; Chen, Z.; Davis, M. F.; Franzen, S. *Acta Crystallogr., Sect. D* **2007**, *D63*, 1094.
(11) LaCount, M. W.; Zhang, E.; Chen, Y. P.; Han, K.; Whitton, M. M.; Lincoln, D. E.; Woodin, S. A.; Lebioda, L. *J. Biol. Chem.* **2000**, *275*, 18712.
(12) de Sorrano, V.; D'Antonio, J.; Thompson, M. K.; Franzen, S.; Ghiladi, R. A. *Acta Crystallogr., Sect. D* **2010**.
(13) D'Antonio, J.; D'Antonio, E. L.; Bowden, E. F.; Smirnova, T.; Franzen, S.; Ghiladi, R. A. *J. Biol. Chem.* **2010**.
(14) Davydov, R.; Osborne Robert, L.; Kim Sun, H.; Dawson John, H.; Hoffman Brian, M. *Biochemistry* **2008**, *47*, 5147.
(15) Smirnova, T. I.; Weber, R. T.; Davis, M. F.; Franzen, S. *J. Am. Chem. Soc.* **2008**, *130*, 2128.
(16) Feducia, J.; Dumarieh, R.; Gilvey, L. B. G.; Smirnova, T.; Franzen, S.; Ghiladi, R. A. *Biochemistry* **2009**, *48*, 995.
(17) Matsui, T.; Ozaki, S.; Liong, E.; Phillips, G. N.; Watanabe, Y. *J. Biol. Chem.* **1999**, *274*, 2838.
(18) Howes, B. D.; Rodriguez-Lopez, J. N.; Smith, A. T.; Smulevich, G. *Biochemistry* **1997**, *36*, 1532.
(19) Lebioda, L.; LaCount, M. W.; Zhang, E.; Chen, Y. P.; Han, K.; Whitton, M. M.; Lincoln, D. E.; Woodin, S. A. *Nature (London)* **1999**, *401*, 445.
(20) de Serrano, V.; D'Antonio, J.; Franzen, S.; Ghiladi, R. A. *Acta Crystallogr., Sect. D* **2010**, *66*, 529.
(21) Franzen, S.; Belyea, J.; Gilvey, L. B.; Davis, M. F.; Chaudhary, C. E.; Sit, T. L.; Lommel, S. A. *Biochemistry* **2006**, *45*, 9085.
(22) Matsui, T.; Ozaki, S.-i.; Watanabe, Y. *J. Biol. Chem.* **1997**, *272*, 32735.
(23) Matsui, T.; Ozaki, S.-i.; Watanabe, Y. *J. Am. Chem. Soc.* **1999**, *121*, 9952.

(24) Sakakura, M.; Morishima, I.; Terazima, M. *Biochemistry* **2002**, *41*, 4837.
(25) Matsui, T.; Ozaki, S.-I.; Liong, E.; Phillips, G. N., Jr.; Watanabe, Y. *J. Biol. Chem.* **1999**, *274*, 2838.
(26) Alayash, A. I.; Ryan, B. A. B.; Eich, R. F.; Olson, J. S.; Cashon, R. E. *J. Biol. Chem.* **1999**, *274*, 2029.
(27) Fenwick, C. W.; English, A. M. *J. Am. Chem. Soc.* **1996**, *118*, 12236.
(28) Tanaka, M.; Ishimori, K.; Mukai, M.; Kitagawa, T.; Morishima, I. *Biochemistry* **1997**, *36*, 9889.
(29) Yang, H. J.; Matsui, T.; Ozaki, S.; Kato, S.; Ueno, T.; Phillips, G. N.; Fuku-Zumi, S.; Watanabe, Y. *Biochemistry* **2008**, *47*, 2700.
(30) Redaelli, C.; Monzani, E.; Santagostini, L.; Casella, L.; Sanangelantoni, A. M.; Pierattelli, R.; Banci, L. *ChemBioChem* **2002**, *3*, 226.
(31) Tanaka, M.; Ishimori, K.; Morishima, I. *Biochem. Biophys. Res. Commun.* **1996**, *227*, 393.
(32) Davis, M. F.; Gracz, H.; Vendeix, F. A. P.; de Serrano, V.; Somasundaram, A.; Decatur, S. M.; Franzen, S. *Biochemistry* **2009**, *48*, 2164.
(33) Otwinowski, Z.; Minor, W. *Methods Enzymol.* **1997**, *276*, 307.
(34) Krissinel, E. B.; Winn, M. D.; Ballard, C. C.; Ashton, A. W.; Patel, P.; Potterton, E. A.; McNicholas, S. J.; Cowtan, K. D.; Emsley, P. *Acta Crystallogr., Sect. D* **2004**, *D60*, 2250.
(35) Potterton, L.; McNicholas, S.; Krissinel, E.; Gruber, J.; Cowtan, K.; Emsley, P.; Murshudov, G. N.; Cohen, S.; Perrakis, A.; Noble, M. *Acta Crystallogr., Sect. D* **2004**, *D60*, 2288.
(36) Emsley, P.; Cowtan, K. *Acta Crystallogr., Sect. D* **2004**, *D60*, 2126.
(37) Phillips, J. C.; Braun, R.; Wang, W.; Gumbart, J.; Tajkhorshid, E.; Villa, E.; Chipot, C.; Skeel, R. D.; Kale, L.; Schulten, K. *J. Comput. Chem.* **2005**, *26*, 1781.
(38) Delley, B. *J. Chem. Phys.* **1990**, *92*, 508.
(39) Delley, B. *J. Chem. Phys.* **2000**, *113*, 7756.
(40) Perdew, J. P.; Burke, K.; Wang, Y. *Phys. Rev. B: Condens. Matter* **1996**, *54*, 16533.
(41) Poulos, T. L.; Kraut, J. *J. Biol. Chem.* **1980**, *255*, 8199.
(42) Fenton, H. J. H. *J. Chem. Soc., Trans.* **1894**, *65*, 899.
(43) D'Antonio, J.; D'Antonio, E. L.; Thompson, M. K.; Bowden, E. F.; Franzen, S.; Smirnova, T.; Ghiladi, R. A. *Biochemistry* **2010**, *49*, 6600.
(44) Nienhaus, K.; Deng, P.; Belyea, J.; Franzen, S.; Nienhaus, G. U. *J. Phys. Chem. B* **2006**, *110*, 13264.
(45) Belyea, J.; Belyea, C. M.; Lappi, S.; Franzen, S. *Biochemistry* **2006**, *45*, 14275.
(46) Franzen, S.; Gilvey, L. B.; Belyea, J. L. *Biochim. Biophys. Acta, Proteins Proteomics* **2007**, *1774*, 121.
(47) Ma, H. A.; Thompson, M. K.; Gaff, J.; Franzen, S. *J. Phys. Chem. B* **2010**, *114*, 13823.
(48) Yang, F.; Phillips, G. N., Jr. *J. Mol. Biol.* **1996**, *256*, 762.
(49) de Serrano, V. S.; Davis, M. F.; Gaff, J. F.; Zhang, Q.; Chen, Z.; D'Antonio, E. L.; Bowden, E. F.; Rose, R.; Franzen, S. *Acta Crystallogr., Sect. D* **2010**, *66*, 770.
(50) Nicoletti, F. P.; Thompson, M. K.; Howes, B. D.; Franzen, S.; Smulevich, G. *Biochemistry* **2010**, ACS Just Accepted.
(51) Thompson, M. K.; Franzen, S.; Ghiladi, R. A.; Reeder, B. J.; Svistunenko, D. A. *J. Am. Chem. Soc.* **2010**, *132*, 17501.
(52) Svistunenko, D. A.; Dunne, J.; Fryer, M.; Nicholls, P.; Reeder, B. J.; Wilson, M. T.; Bigotti, M. G.; Cutruzzola, F.; Cooper, C. E. *Biophys. J.* **2002**, *83*, 2845.
(53) Meno, K.; Jennings, S.; Smith, A. T.; Henriksen, A.; Gajhede, M. *Acta Crystallogr., Sect. D* **2002**, *58*, 1803.
(54) Wan, L. L.; Twitchett, M. B.; Eltis, L. D.; Mauk, A. G.; Smith, M. *Proc. Natl. Acad. Sci. U.S.A.* **1998**, *95*, 12825.
(55) Davydov, R.; Osborne, R. L.; Shanmugam, M.; Du, J.; Dawson, J. H.; Hoffman, B. M. *J. Am. Chem. Soc.* **2010**, *132*, 14995.
(56) Sitter, A. J.; Shifflett, J. R.; Terner, J. *J. Biol. Chem.* **1988**, *263*, 13032.
(57) Smith, A. T.; Veitch, N. C. *Curr. Opin. Chem. Biol.* **1998**, *2*, 269.
(58) Vitello, L. B.; Erman, J. E.; Miller, M. A.; Wang, J.; Kraut, J. *Biochemistry* **1993**, *32*, 9807.
(59) Bonagura, C. A.; Bhaskar, B.; Shimizu, H.; Li, H.; Sundaramoorthy, M.; McRee, D. E.; Goodin, D. B.; Poulos, T. L. *Biochemistry* **2003**, *42*, 5600.
(60) Gajhede, M.; Schuller, D. J.; Henriksen, A.; Smith, A. T.; Poulos, T. L. *Nat. Struct. Biol.* **1997**, *4*, 1032.
(61) Mukai, M.; Nagano, S.; Tanaka, M.; Ishimori, K.; Morishima, I.; Ogura, T.; Watanabe, Y.; Kitagawa, T. *J. Am. Chem. Soc.* **1997**, *119*, 1758.
(62) Phillips, G. N.; Arduini, R. M.; Springer, B. A.; Sligar, S. G. *Proteins: Struct., Funct., Genet.* **1990**, *7*, 358.
(63) Ghiladi, R. A.; Medzihradszky, K. F.; Ortiz de Montellano, P. R. *Biochemistry* **2005**, *44*, 15093.
(64) Heering, H. A.; Indiani, C.; Regelsberger, G.; Jakopitsch, C.; Obinger, C.; Smulevich., G. *Biochemistry* **2002**, *41*, 9237.
(65) Huyett, J. E.; Doan, P. E.; Gurbiel, R.; Houseman, A. L. P.; Sivaraja, M.; Goodin, D. B.; Hoffman, B. M. *J. Am. Chem. Soc.* **1995**, *117*, 9033.
(66) Pond, A. E.; Bruce, G. S.; English, A. M.; Sono, M.; Dawson, J. H. *Inorg. Chim. Acta* **1998**, *275*−*276*, 250.
(67) Sturgeon, B. E.; Battenburg, B. J.; Lyon, B. J.; Franzen, S. *Chem. Res. Toxicol.* **2011**, *24*, 1862.
(68) Badyal, S. K.; Eaton, G.; Mistry, S.; Pipirou, Z.; Basran, J.; Metcalfe, C. L.; Gumiero, A.; Handa, S.; Moody, P. C. E.; Raven, E. L. *Biochemistry* **2009**, *48*, 4738.
(69) Laskowski, R. A.; MacArthur, M. W.; Moss, D. S.; Thornton, J. M. *J. Appl. Crystallogr.* **1993**, *26*, 283.